Energy and angular distribution of electrons ejected from autoionization states in helium by electron impact

N. Oda, S. Tahira,* and F. Nishimura

Research Laboratory of Nuclear Reactor, Tokyo Institute of Technology, Meguro-ku, Tokyo, Japan

F. Koike

Department of Physics, School of Medicine, Kitasato University, Sagamihara, Kanagawa, Japan
(Received 9 September 1976)

Energy spectra of electrons ejected from autoionization states in helium by electron impact have been extensively measured for primary energies from 65 to 1000 eV and for ejection angles from 13° to 142°. The line shape in energy spectra undergoes a noticeable change with ejection angle as well as impact energy, reflecting the characteristics of the corresponding autoionization state. The single differential cross sections (differential in angle) for emissions of autoionized electrons have been obtained by integrating the energy spectra in the vicinity of each isolated resonance with respect to the energy after subtraction of the continuum background, for the $(2s^2)^1S$, $(2s2p)^3P$, $(2p^2)^1D$, and $(2s2p)^1P$ states as a function of primary energy at 33°, 127°, and 142°. Profiles of the spectra due to the $(2s^2)^1S$ state have been analyzed using Fano's formula, and the shape parameter q is given as a function of ejection angle for 250-eV impact. A number of the autoionization states lying above ~ 62 eV have also been measured and identified as members of the $(2sns)^1S$, $(2pnp)^1S$, $(sp2n-)^3P$, $(2pnp)^1D$, and $(sp2n+)^1P$ $(n = 2\text{–}5)$ series, and our results are compared with previous results of theory and experiment.

I. INTRODUCTION

The autoionization states in helium have been investigated experimentally by several methods; i.e., optical absorption spectrum measurements,[1] electron energy-loss measurements of forward scattered electrons,[2-6] energy spectrum measurements of electrons ejected from states excited by ion[7-19] and electron impact,[20-26] the trapped electron method,[27-29] optical emission spectrum measurements,[30, 31] and ionization yield measurements by electron impact.[32] Detailed measurements of the doubly differential (differential in angle and in energy) cross sections for the electrons ejected by electron impact are, however, still important and interesting from several points of view. First, it should be worthwhile to compare the precise experimental data of the energy positions and the widths of the autoionization states with the recently calculated theoretical values. Second, such experiments provide important information about a correlation effect in the ground state of helium as was discussed by Wiebes[33] and also provide basic data for the difference between the excitation mechanisms by electron, heavy-charged-particle, and photon impact. Third, interesting information will be obtained for the mechanism of spin-forbidden triplet excitations in moderate- and low-impact-energy regions. A transition from the ground state (with spin zero) to the triplet state (with spin 1) can only be accomplished by interchanging an electron from an impinging particle with one of the orbital electrons of helium. For instance, a molecular hydrogen ion H_2^+ can excite that state but a proton cannot, whereas an impinging electron itself can exchange with one of the bound electrons. A comparison between excitation cross sections by electron, H^+, H_2^+, and He impacts has already been made.[34]

Regarding the theoretical calculations, intensive studies have been made of the autoionization from helium atoms by Lipovetsky and Senashenko.[35] Their theory is based on the Born approximation. They have calculated the doubly differential cross sections for several autoionizing peaks and the resonance profile parameters for $He(2s^2)^1S$ and $He(2s2p)^1P$ autoionization states, and have revealed that considerable variations of the profile of $He(2s^2)^1S$ resonance with ejection angle are due to a strong interference between the components with different angular momenta of the transition amplitudes. Jacobs[36] also has made similar calculations and obtained the resonance profile parameters for the lowest-lying ^1S, ^1P, and ^1D states by fitting the Fano-Beutler function to his calculated energy spectra.

In a previous letter,[21] a part of the measurements of the energy and angular distributions of electrons ejected from autoionization states in helium by electron impact was described. In this paper, a more complete account of the experimental procedure and the experimental results which cover extensively the wide regions of the energy of incident electrons and of the ejection angle are given. Besides the above, a number of autoionizing levels lying above $\sim$62 eV in helium, some of which were

first observed by the H_2^+ impact,[7] have been ob-
served and identified. Recently, not a little atten-
tion was paid to the threshold effect for the autoion-
ization states excited by electron impact at impact
energies slightly above the threshold energy.[37]
However, this subject is excluded in this paper
and incident energies are chosen in the energy
region sufficiently higher than the threshold value.

II. EXPERIMENTAL APPARATUS AND PROCEDURE

The experimental apparatus is schematically
shown in Fig. 1.[38] The vacuum system is subdivid-
ed into three regions: electron gun chamber
A; target gas chamber B; electron analyzer cham-
ber C. These regions are separately pumped by
two series of diffusion pump systems with molecu-
lar sieve traps. When the vacuum system is
baked out at about 200 ℃ for 4–5 h, the base pres-
sure of 3×10^{-9} Torr can be attained in the target gas
chamber. The target gas is fed into the target gas
chamber through a pipe with an automatic variable
leak valve from a gas reservoir. The target gas
is, after being purified through a molecular sieve
cooled with liquid nitrogen, filled to a pressure of
200–300 Torr in the gas reservoir. The purity of
the gas is continuously monitored by a quadrupole
residual gas analyzer. The target gas pressure
was measured with a MKS-Baratron membrane
manometer. When the pressure in the target
chamber is, for example, 2×10^{-3} Torr, the pres-
sure in the gun chamber and in the analyzer cham-
ber is $\sim 1 \times 10^{-5}$ Torr. The working target gas

FIG. 1. Schematic drawing of the apparatus: F, fila-
ment; L_1, collimation lens; A_1, exit aperture; A_2, en-
trance aperture; P, collision center; L_2, retardation
lens; L_3, Einzel lens; L_4, L_5, cylindrical lenses. For
the definition of the other symbols in figure, see the
text.

pressure was 1×10^{-4}–1×10^{-3} Torr.

Primary electrons emitted from a tungsten fila-
ment F, after being collimated by a lens L_1, enter
the target gas chamber through a 1-mm-diam exit
aperture A_1. The beam profile as well as the beam
energy spectrum are measured with either the
Faraday cup or the electron energy analyzer. The
primary beam energy was varied from 65 to 1000
eV and the beam current was 20–100 μA in this
measurement. The beam diameter at the collision
center P was about 2 mm. The energy spread of
the beam was ~0.6 eV full width at half maximum
(FWHM). The Faraday cup consists of three parts:
a collector C, a retarding potential energy analyz-
er R consisting of three electrodes, and a gold-
plated tungsten 98% transmission mesh G. The
fluctuation of the beam was kept constant to less
than ±1% for each run, and the beam intensity was
measured prior to and after every angle setting of
the analyzer.

Electrons ejected from a small collision volume
around the collision center P enter the analyzer
chamber through a 1-mm-diam aperture A_2. The
energy analyzer can be rotated from outside over
an angular range from −90° to +145° with respect
to the primary beam. The analyzing system con-
sists of four components: (i) a retardation lens
L_2 (slits S_1, S_2, and S_3), (ii) an Einzel lens L_3
(slits S_3 and S_4, and electrodes D_1 and D_2), (iii) a
90° electrostatic cylindrical analyzer, and (iv)
acceleration lenses, L_4 and L_5. The slit S_5 is
used as the Herzog electrode. For the 90° cylin-
drical analyzer adopted here, the defining entrance
and exit slits are, in the zero approximation, S_3
and S_6, respectively, and heights of both slits
were varied from 0.1 to 0.4 mm according to the
required energy resolution. All the slits of the
analyzing system S_1 to S_6 are of the rectangular
and knife-edge shape.

The measured angular resolution (FWHM) of
the detection system was ~2° which is close to the
value expected from the analyzing geometry. The
incoming electrons are decelerated to a constant
analyzing energy, typically ~10 eV, by varying the
voltage applied to the retardation lens and then
are energy analyzed with a constant-energy resolu-
tion. For the energy range of ejected electrons
measured in this experiment, the transmission of
the analyzing system could be kept nearly constant
in spite of the deceleration by applying appropriate
voltages to the retardation lens and the Einzel
lens, where the same voltage was applied to S_3,
S_4, S_5, and S_6.

The radii of the inner and outer electrodes of
the 90° cylindrical analyzer are 22 and 28 mm (G_1
and G_2), respectively. Each of the inner and outer
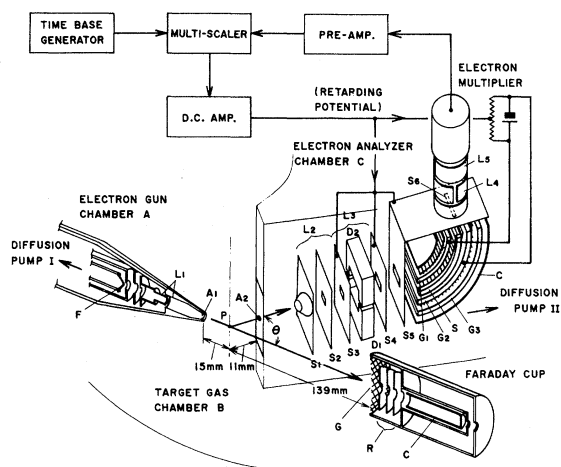electrodes is made to form a double grid by stringing

0.05-mm tungsten wire on the frames. Further-
more, another grid (G_3) of the same structure as
G_1 and G_2 is set outside G_2 to act as a suppressor
grid for the higher energy electrons reflected from
the outer collector C. A pair of side repeller
electrodes (S) is set in parallel to each other in
the space between G_1 and G_2.

Electrons emerging from the exit slit S_6 of the
analyzer are collimated and accelerated to a con-
stant energy of 330 eV by two rows of cylindrical
lenses $(L_4$ and $L_5)$, and finally strike the first dy-
node of an electron multiplier (EMI-9707). All
electrodes and grids of the analyzing system are
gold plated.

The residual magnetic field in the main part of
the apparatus, was annulled to below about 5 mG
by means of two mutually perpendicular pairs of
2-m-square Helmholtz coils and double layers of
permalloy shields.

The energy-selected electrons are detected by
the electron multiplier and the output pulses are
amplified and stored in a multiscaler. The re-
tarding voltage applied to the retardation lens is
generated by converting the channel address of
the multiscaler to an analog voltage by the use of
the D-A converter, so that the channel advance of
the multiscaler is synchronized with the retarding
voltage to within an accuracy of ~ 0.01 eV. The
sweeping range of the retarding voltage was in this
measurement at most 10 V.

The energy of measured electrons, E_{kin}, is given
by

$$E_{kin} = V_r + f V_d , \qquad (1)$$

where V_r is the retardation voltage, V_d is the po-
tential difference between the inner and the outer
cylindrical electrodes, and f is the analyzer con-
stant determined from the radii of cylindrical
electrodes. The energy E_{kin}, derived from the
measurement of V_r, is often different from the
true value, because of (1) energy shift due to the
contact potential, and (2) electric potential caused
by space charge in the collision space. Therefore,
the energy spectra measured as a function of V_r
must be calibrated in the energy scale. The en-
ergy difference between two Auger peaks $M_4N_1N_{2,3}$
and $M_5N_1N_{2,3}$ in krypton, which were measured in
an auxiliary run, was compared with the energy
difference obtained from optical data.[39] The en-
ergy difference obtained by the present energy
analyzer were in good agreement with the optical
data within an accuracy of 0.01 eV. Thus, the en-
ergy difference between two different positions of
energy spectra can be measured within this ac-
curacy. In order to calibrate the energy scale ab-
solutely, the 60.130-eV value for the $(2s2p)^1P$ lev-

el measured by Madden and Codling[1] was used to
calibrate one point of the energy scale.

When the collision chamber was evacuated,
background counts were negligibly few except in
the neighborhood of the forward direction. The
experimental results in the directions below 10°
were corrected for background counts. Prior to
each set of measurement, the position of zero
angle was found by determining the position of
equal current on either side of the incident elec-
tron beam, and also by measuring the electrons
elastically scattered from the target gas on either
side with respect to the electron beam. Except
for angles larger than 90°, the electrons were
measured at both $+\theta$ and $-\theta$ to confirm the sym-
metry of scattering. The absolute value of angular
position θ could be determined within an accuracy
$\sim 1°$, and the relative one within an accuracy $\sim 0.5°$.

III. RESULTS AND DISCUSSION

A. Dependence of the energy spectra on the energy of primary electrons

The energy spectra of autoionized electrons in
the backward direction are shown in Figs. 2 and 3
as a function of the energy E_0 of primary elec-
trons. The energy spectra of secondary electrons
measured here contain the continuum spectra re-
sulting from the direct ionization in addition to
the line spectra due to autoionization.[40] In Figs.
2 and 3, the energy of autoionized electrons can be
obtained by subtracting the first ionization poten-
tial (24.58 eV) from the excitation energy. The
energy spectra shown in Fig. 2[41] were observed at
142° with an energy resolution of 0.15 eV and in-
volve the whole energy region of autoionization
states which converge to the $He^+(n=2)$ state. Fig-
ure 3 shows the energy spectra with higher reso-
lution of 0.08 eV in the energy region near 60 eV,
observed at 127°. The energy spectra of auto-
ionized electrons in the forward direction are
shown in Fig. 4 as a function of the primary en-
ergy, where the ejection angle is 33° and the en-
ergy resolution is 0.08 eV. Since the energy
spectra given in Figs. 2–4 are shown in arbitrary
scales and differential in energy and angle of
ejected electrons, these spectra can be called
the relative doubly differential cross sections
(hereafter, abbreviated as relative DDCS's) for
the ejected electrons which are composed of the
directly ionized electrons and the autoionized
electrons. The former part of the ejected elec-
trons gives a continuum part of energy spectra
and was measured by Opal et al.[42-44] and Oda et
al.[40] Referring to Figs. 2–4, the following fea-
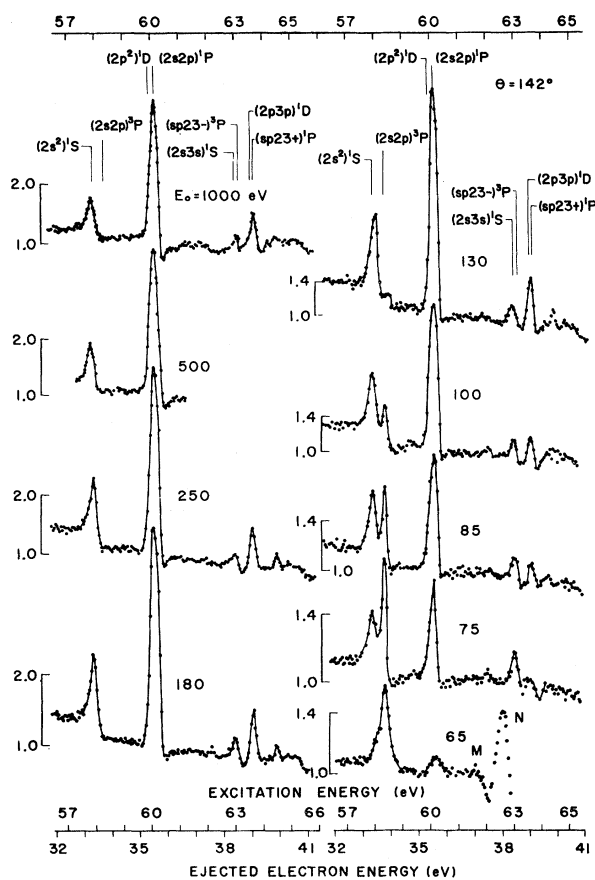tures are noted.

FIG. 2. Energy spectra of autoionized electrons; dependence on impact energy E_0; energy resolution of electron energy analyzer is 0.15 eV in FWHM. Ejection angle is 142°. Structures, M and N, are due to electrons scattered inelastically by helium (Ref. 41). Intensity of continuum at the energy of $(2s2p)^1P$ state is normalized to 1.0 and the length corresponding to the intensity scale is shown on the left-hand side of each spectrum.

FIG. 3. Details of dependence on impact energy in neighborhood of 60-eV excitation energy. Energy resolution $(\Delta E_{1/2})$ is 0.08 eV in FWHM. Ejection angle is 127°.

1. The energy spectra in the backward direction:
Figs. 2 and 3. (a) All the line shapes of the energy spectra are nearly peaklike and remain almost invariant as the primary energy is varied. (b) The peaks for the optically forbidden states, $(2s^2)^1S$ and $(2p^2)^1D$, are intensely visible over the whole primary energy range except for the lowest energy 65 eV, even at the highest primary energy 1000 eV. (c) The peak height for the $(2s2p)^3P$ state is most prominent when the primary energy approaches the excitation threshold of this state (58.3 eV) and decreases rapidly with the increase of the primary energy. This trend is consistent with the general shape of the excitation function of the spin forbidden triplet state. (d) The peak for the $(2p^2)^1D$ state is well separated from that for the neighboring $(2s2p)^1P$ over the whole pri-
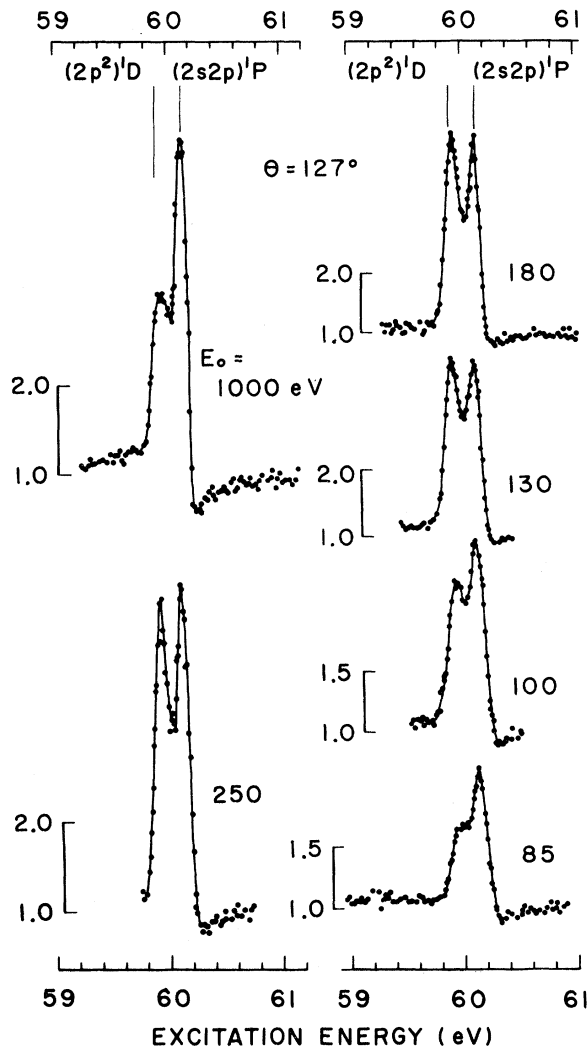
mary energy range and the difference in energy between two peaks is 0.20 eV for 180-eV electron impact (Fig. 3).

2. The energy spectra in the forward direction:
Fig. 4. (a) Although the line shapes for the $(2p^2)^1D$ and $(2s2p)^1P$ are almost peaklike in most of energy spectra, the line shape for the $(2p^2)^1D$ becomes diplike when the primary energy is increased to higher energies, e.g., 1000 eV. (b) The line shape for the $(2s^2)^1S$ state at 33° varies from symmetrical at the low energies to a pronounced asymmetry at the higher energies. (c) The peak for the $(2p^2)^1D$ state is almost completely separated from that for the $(2s2p)^1P$ state. The difference between two peaks is 0.23 eV for 180-
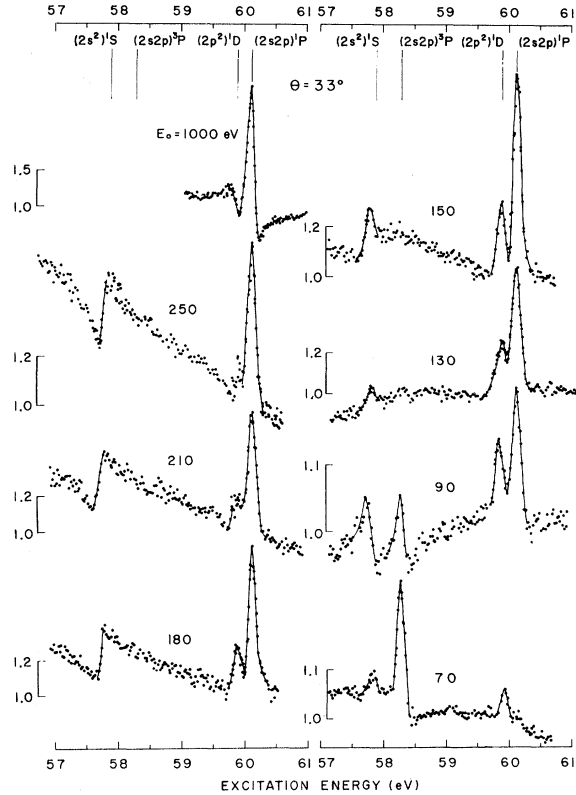
FIG. 4. Energy spectra of autoionized electrons: dependence on impact energy. Ejection angle is 33°; $\Delta E_{1/2} = 0.08$ eV.

eV electron impact, which is larger than that in the backward direction, i.e., 0.20 eV. (d) The peak for the $(2s2p)^3P$ state becomes most prominent at the primary energy close to the threshold energy in the same way as for the backward directions.

B. Dependence of the energy spectra on the ejection angle

The energy spectra of autoionized electrons ejected by 250-eV primary electrons are shown in Fig. 5, which were observed with an energy resolution of 0.15 eV and involve the whole energy region of autoionization states converging to the energy of He$^+$($n = 2$) state. The energy spectra due to $(2s^2)^1S$ state in Fig. 5 are most useful for the line-shape analysis, because the structure due to the neighboring states such as $(2s2p)^3P$ state does not disturb the above analysis for this primary energy.

The energy spectra due to $(2s^2)^1S$ state were analyzed using Fano's formula.[45] This formula takes the following form,

$$\sigma(\epsilon) = \sigma_a \frac{(q+\epsilon)^2}{1+\epsilon^2} + \sigma_b , \qquad (2)$$
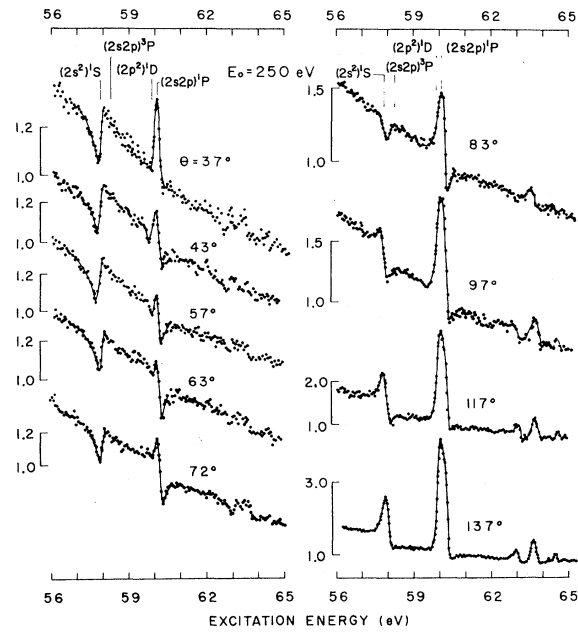

FIG. 5. Energy spectra of autoionized electrons. Impact energy is 250 eV; dependence on ejection angle; $\Delta E_{1/2} = 0.15$ eV.

where

$$\epsilon = (E - E_r)/\tfrac{1}{2}\Gamma , \qquad (3)$$

and E_r and Γ are the resonance energy and the resonance width, respectively. σ_a and σ_b are a resonant and a nonresonant part of the DDCS $\sigma(\epsilon)$, respectively. Cross section $\sigma(\epsilon)$ given in Eq. (2) was originally derived for the photon absorption cross section,[45] which represents the total excitation cross section. Lipovetsky and Senashenko[35] have shown, using the Born approximation, that this type of cross-section formula is also applicable to the autoionized electrons. In the present analysis, it is assumed that the form given in Eq. (2) is also applicable to the energy spectra of autoionized electrons. Therefore, the meaning of q in the present application is probably different from that given by Fano. Since the energy spectra were measured with the energy resolution $\Delta E_{1/2}$, which is comparable with or larger than the natural width Γ of autoionization states, the theoretical spectrum is expressed by

$$y(E; q, \rho^2, E_r, \Gamma)$$

$$= \int_0^\infty \left(\sigma_a(E') \frac{[q + (E' - E_r)/\tfrac{1}{2}\Gamma]^2}{1 + (E' - E_r)/\tfrac{1}{2}\Gamma} + \sigma_b(E') \right)$$

$$\times \frac{1}{\delta\sqrt{2\pi}} \exp\left[-\left(\frac{E' - E}{\delta\sqrt{2}} \right)^2 \right] dE' , \qquad (4)$$

where σ_a and σ_b are assumed to be linear functions of E'. The exponential term yields the instrumental spread of natural line shape and $\delta = \Delta E_{1/2} / [2(2\log 2)^{1/2}]$. The parameter ρ^2 is defined by

$$\rho^2 = \sigma_a / (\sigma_a + \sigma_b) \qquad (5)$$

and is assumed to be independent of E' in the neighborhood of the resonance energy. The theoretical spectra based on Eq. (4) are fitted to experimental ones given in Fig. 5 with the adjustable parameters, q and ρ^2, where for E_r and Γ were assumed theoretical values.[46] The q and ρ^2 values for 250-eV electron impact are shown in Figs. 6 and 7, respectively, as a function of the ejection angle. The error bars in Figs. 6 and 7 show the standard deviations of parameters due to the fitting procedure and the experimental errors may be estimated to be less than ~2%.

In Fig. 6 are also shown the theoretical q values by Lipovetsky and Senashenko[35] and the experimental ones by Suzuki et al.,[24] for 400-eV electron impact. The experimental q values decrease monotonically with ejection angle and the sign of q value changes near 90°. The theoretical values
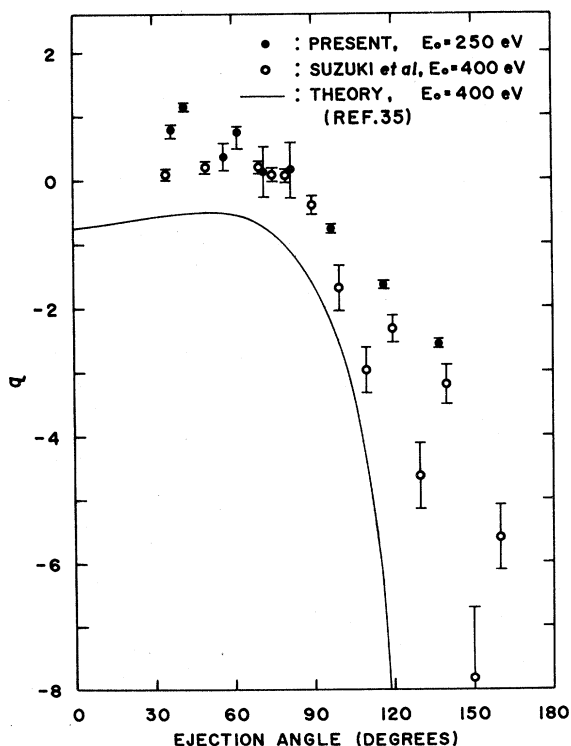

FIG. 6. Line-shape parameter q as a function of angle, for the $(2s^2)^1S$ state in helium: closed circles, present results, 250-eV electron impact; open circles, 400-eV electron impact, measured by Suzuki et al. (Ref. 24); solid line, 400-eV electron impact, Born approximation calculation by Lipovetsky and Senashenko (Ref. 35).
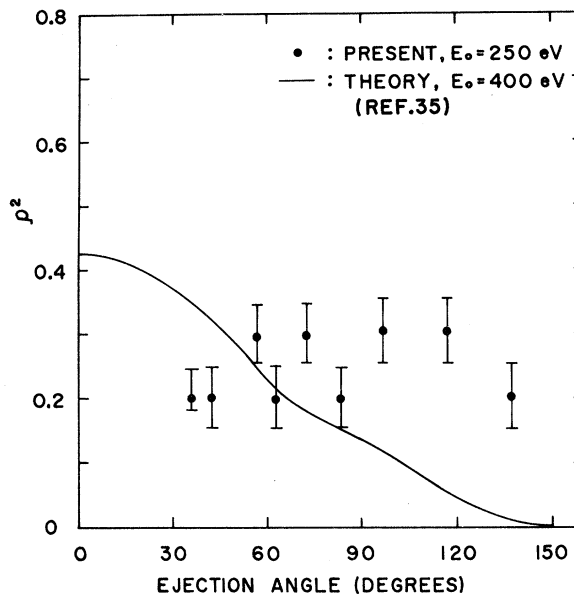

FIG. 7. ρ^2 value as a function of angle, for the $(2s^2)^1S$ state in helium. ρ^2 is defined in Eq. (5). Closed circles, present results, 250-eV electron impact; solid line, 400-eV electron impact, Born approximation calculation by Lipovetsky and Senashenko (Ref. 35).

cannot be compared directly with our experimental ones, because the impact electron energies differ. However, the general tendency is in a fairly good agreement between experiment and theory over the whole angular range measured. In Fig. 7 are also shown the theoretical ρ^2 values by Lipovetsky and Senashenko[35] for 400-eV electron impact. The experimental ρ^2 values are about 0.2–0.3 over the whole angular range, whereas the theoretical ones decrease with ejection angle, becoming ~0.02 at 135°. The agreement between theory and experiment is not good especially for the backward angles. Experimental evidence shows that ρ^2 does not become as small as 0.02 even for the backward angles. The parameter ρ^2 can be expressed by the ratio of the depth σ_a of the resonance dip from the continuum background level $\sigma_a + \sigma_b$ to the background level $\sigma_a + \sigma_b$ of the line profiles in the energy spectra. One can see nonvanishing resonance dips on the high energy side of the resonance profiles, at 137° for 250-eV electron impact in Fig. 5 and also for higher energies at 142° in Fig. 2. This fact suggests that the disagreement is principally due to the invalidity of the theory for the extreme angular ranges. A more precise and detailed theoretical study would be desirable.

The energy spectra of autoionized electrons by 1000-eV electron impact are shown in Figs. 8(a) and 8(b) as a function of the ejection angle. The
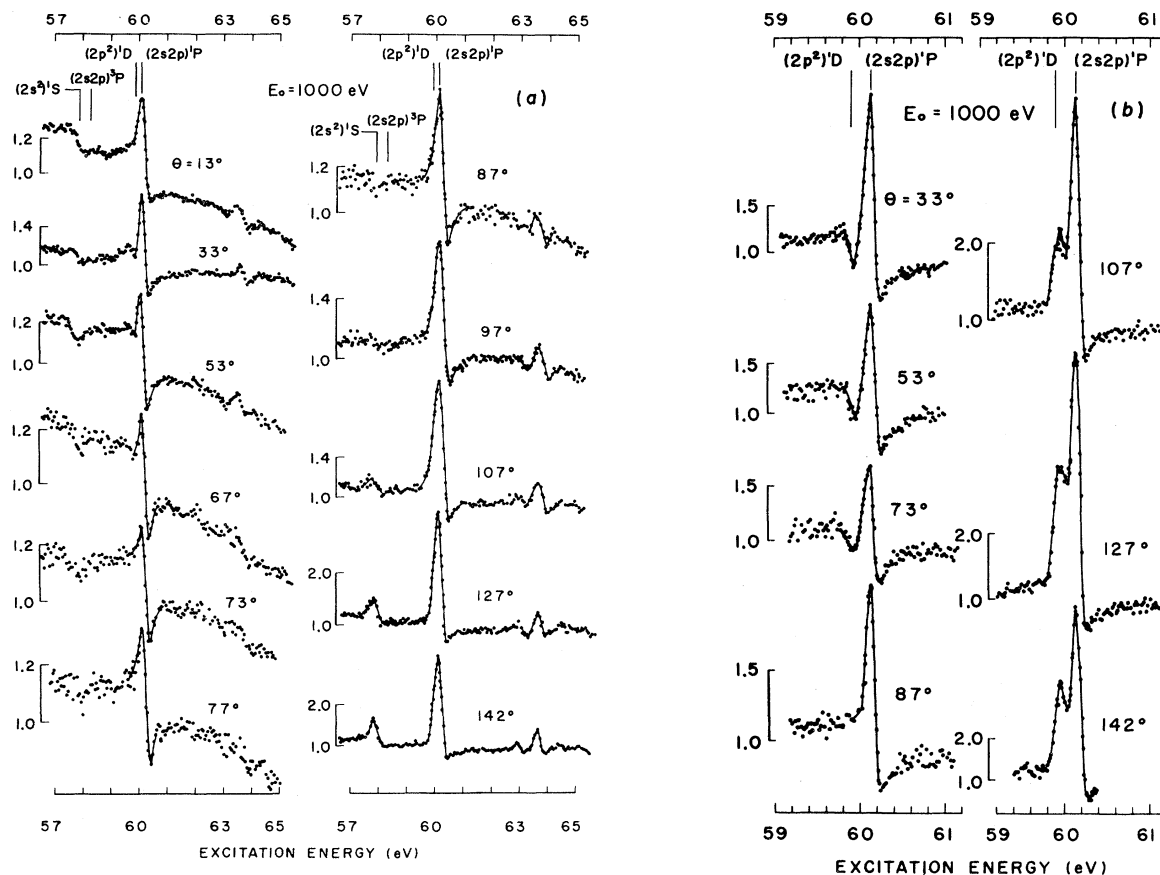
FIG. 8. Energy spectra of autoionized electrons. Impact energy is 1000 eV; dependence on ejection angle: (a) $\Delta E_{1/2}$ =0.15 eV; (b) $\Delta E_{1/2}$=0.08 eV.

energy spectra shown in Fig. 8(a) were observed with an energy resolution of 0.15 eV and involve the whole energy region of autoionization states which converge to the energy of $He^+(n=2)$ state. Figure 8(b) shows the results of a more detailed investigation with higher resolution of 0.08 eV in the energy region near 60 eV. The energy spectra of autoionized electrons by 180- and 85-eV electron impacts are shown in Figs. 9 and 10 as a function of the ejection angle. The most prominent feature seen in these results is that the line shape of energy spectra undergoes a noticeable change with the ejection angle. The principal features of the observed angular distributions are as follows.

1000-eV impact: Fig. 8(a), $\Delta E_{1/2} = 0.15$ eV; 8(b),

$$\Delta E_{1/2} = 0.08 \ eV$$

(a) At smaller angles, dips are seen in both sides of a single peak in the excitation energy region near 60 eV. With an increase of the angle,

the dip on the low-energy side changes to a peak. It was confirmed from the auxiliary experiment utilizing the helium gas mixed with krypton gas that the position of the peak on the high-energy side remains unchanged over the whole range of angles. Thus it was verified that peaks and dips on the high-energy side near 60 eV are due to the same state, namely, $(2s2p)^1P$ state, whereas the structure on the low-energy side is due to the $(2p^2)^1D$ state.

(b) The energy spectra due to the $(2s^2)^1S$ state are diplike and less noticeable in the forward and intermediate angular ranges. In the backward direction, the $(2s^2)^1S$ state becomes more prominent and exhibits a peaklike line shape.

180-eV electron impact: Fig. 9, $\Delta E_{1/2} = 0.08$ eV

(a) The dip on the high-energy side of the peak due to the $(2s2p)^1P$ state is evident in the intermediate angular range and becomes less noticeable both in the forward and backward directions.
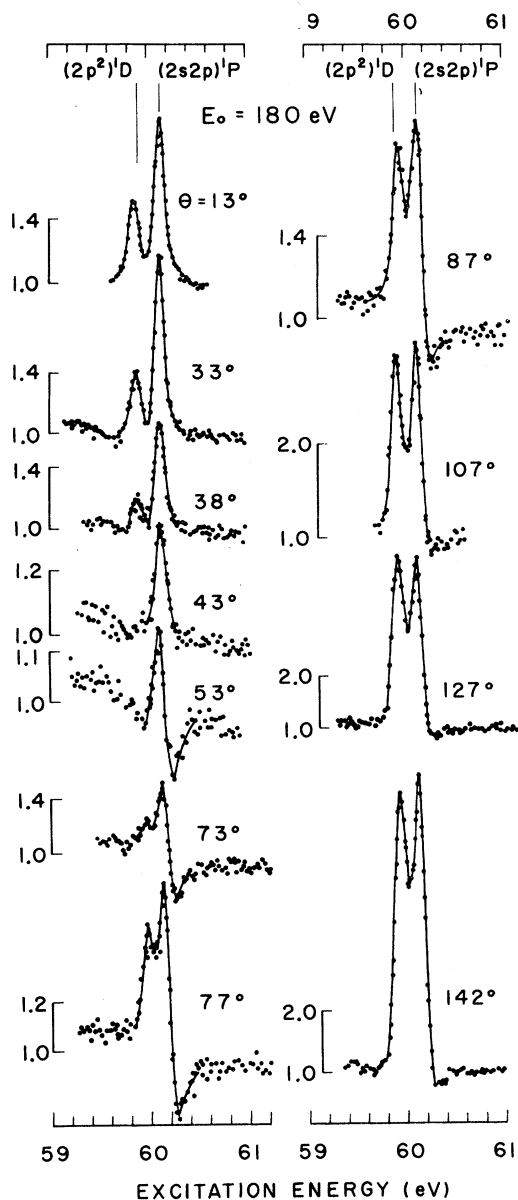
FIG. 9. Details of dependence on ejection angle near 60-eV excitation energy. Impact energy is 180 eV. $\Delta E_{1/2} = 0.08$ eV.

(b) The spectra due to the $(2p^2)^1D$ state show the peaklike line shape in the forward direction and the resonance peak height due to $(2p^2)^1D$ relative to that due to $(2s2p)^1P$ state decreases with increasing angle up to about 38°. The spectra due to the $(2p^2)^1D$ state exhibit the diplike line shape once in the intermediate angular region but again become peaklike above about 70°. The difference in energy between the peak due to the $(2p^2)^1D$ state and that due to the $(2s2p)^1P$ state is 0.23 eV in

the forward direction and 0.20 eV in the backward direction as mentioned before.

85-eV electron impact: Fig. 10(a), $\Delta E_{1/2} = 0.15$ eV; 10(b), $\Delta E_{1/2} = 0.08$ eV

(a) While the spectra due to the $(2s^2)^1S$ state have the diplike line shape at angles below 100° and the peaklike shape above 100°, the spectra due to the $(2s2p)^3P$ state are nearly peaklike over the whole angular range. The resonance peak height due to $(2s2p)^3P$ is almost equal to that due to $(2s^2)^1S$ at 145°, decreases rapidly with decreasing angle down to 110°, and again becomes prominent at angles below 100°.

(b) The spectra due to $(2s2p)^1P$ are peaklike over almost the whole angular range except at 50° and 70°, where dips on the high-energy side of peaks are noticeable. The resonance peak height due to the $(2s2p)^1P$ state has a minimum around 100° as compared with the other resonance peak heights.

(c) The difference in energy between the peak due to the $(2s2p)^1P$ state and that due to $(2p^2)^1D$ varies with the ejection angle in a complicated manner. The maximum value for this difference is 0.28 eV at 40°, but, in general, two peaks approach each other, making it impossible to resolve these two peaks at several angles.

As the resonance energy E_r is connected with the peak energy E_{max} by a relation, $E_r = E_{max} - \Gamma/2q$, the E_{max} value approaches the E_r value if the q value is large. As seen from Fig. 9, both of the line profiles due to ^1D and ^1P states are nearly Lorentzian at 13° and 33°. The resonance energy E_r for $(2p^2)^1D$ state was derived from the spectra at 13° and 33°, using the E_r value for $(2s2p)^1P$, 60.13 eV. The energy width Γ was also derived assuming the Lorentzian line shape for the spectra observed at 13° and 33° (Fig. 10). The E_r and Γ values of the $(2p^2)^1D$ state are $E_r = 59.89 \pm 0.02$ eV, $\Gamma = 0.08 \pm 0.02$ eV. The E_r and Γ values for $(2p^2)^1D$ state were calculated theoretically by several workers.[46-54] Theoretical values of Γ, ranging from 0.06 to 0.08 eV, agree well with our measured value as well as experimental value 0.072 ± 0.018 eV of Hicks and Comer.[26] While some of the theoretical values for E_r are rather larger than the experimental one, the value in Ref. 52 (59.911 eV) and that in Ref. 53 (59.902 eV) agree very well with the measured one.

C. Single differential cross sections

The relative DDCS in the present measurements was put on an absolute scale by comparing the intensity of its continuum part $I_c(E, \theta)$, where E is
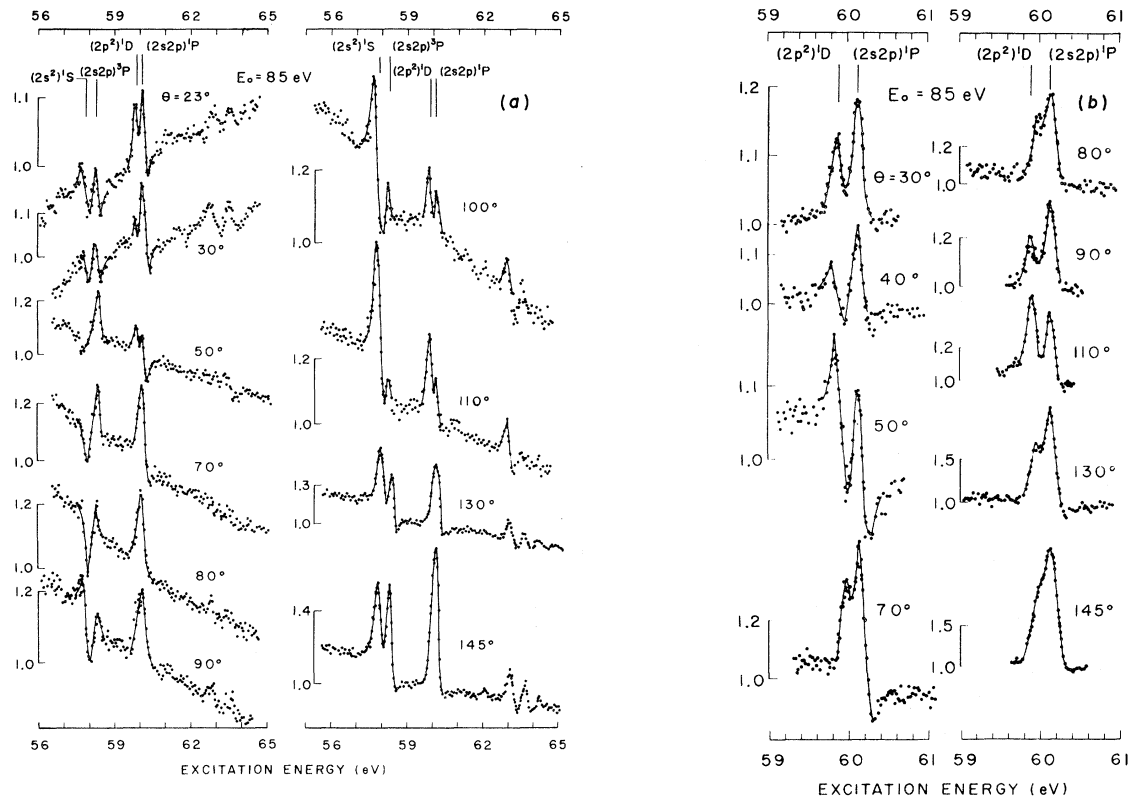
FIG. 10. Energy spectra of autoionized electrons. Impact energy is 85 eV; dependence on ejection angle: (a) $\Delta E_{1/2} = 0.15$ eV; (b) $\Delta E_{1/2} = 0.08$ eV.

the energy of the ejected electron and θ is the ejection angle, with the absolute DDCS for the secondary electrons $\sigma_c(E, \theta)_{op}$ measured by Opal et al.[42-44] The absolute DDCS $\sigma(E', \theta)$ is then given by

$$\sigma(E', \theta) = [\sigma_c(E, \theta)_{op}/I_c(E, \theta)] I(E', \theta), \quad (6)$$

where $I(E', \theta)$ is the intensity of the ejected electrons in the present measurements and the energy variable E' may include the resonance region. A procedure to obtain the DDCS for continuum electrons by using higher-energy resolution and separating the resonance structure from the continuum part was given in Ref. 40. Following this procedure, the energy variable E in $I_c(E, \theta)$ was selected in such a way that the angular distributions measured by Opal et al. have the same form as ours at the energy E. The absolute values of DDCS's thus obtained are believed to be reliable within an accuracy of 20–30%, taking into consideration errors inherent in the continuum DDCS's by Opal et al. and those added by the present normalization procedure. The relative intensities of different energy spectra are reliable
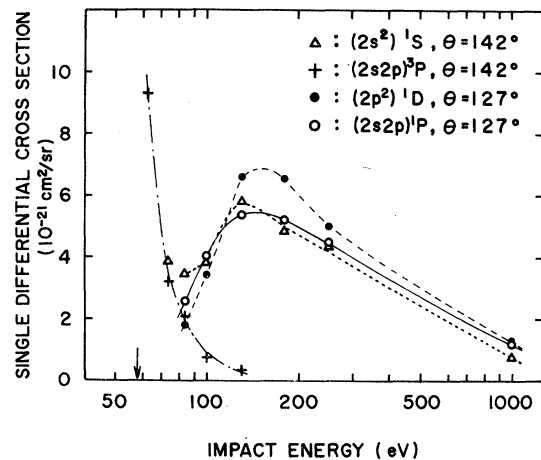

FIG. 11. Single differential cross sections (differential in angle only) for the autoionization states in helium produced by electron impact as a function of impact energy: triangles, $(2s^2)^1S$, ejection angle $\theta = 142°$; crosses, $(2s2p)^3P$, $\theta = 142°$; closed circles, $(2p^2)^1D$, $\theta = 127°$; open circles, $(2s2p)^1P$, $\theta = 127°$. The arrow on abscissa stands for the level energy for the $(2s2p)^3P$ (58.3 eV).
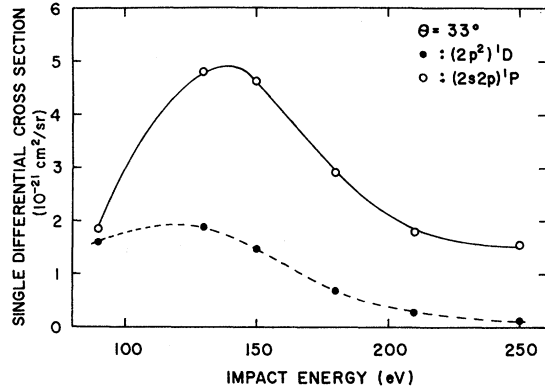
FIG. 12. Single differential cross sections as a function of impact energy: closed circles, $(2p^2)^1D$, $\theta = 33°$; open circles, $(2s2p)^1P$, $\theta = 33°$.

within an accuracy of ~10%.

The single differential cross sections for the emission of autoionized electrons (differential in angle only) $\sigma(\theta)$ were obtained by integrating the absolute DDCS $\sigma(E, \theta)$ after subtracting the continuum background. The single differential cross section $\sigma(\theta)$ in the vicinity of an isolated resonance, in terms of the parameters in Eq. (2), is given by

$$\sigma(\theta) = \int \{\sigma(E, \theta) - [\sigma_a(E, \theta) + \sigma_b(E, \theta)]\} dE$$

$$= \tfrac{1}{2}\pi \Gamma \sigma_a (q^2 - 1), \tag{7}$$

where $\sigma_a(E, \theta) + \sigma_b(E, \theta)$ is the continuum background.

TABLE I. Single differential cross sections (differential in angle only) for the autoionization states $[(2s^2)^1S$, $(2s2p)^3P$, $(2p^2)^1D$, and $(2s2p)^1P]$ in helium as produced by electron impact at energies from 65 to 1000 eV.

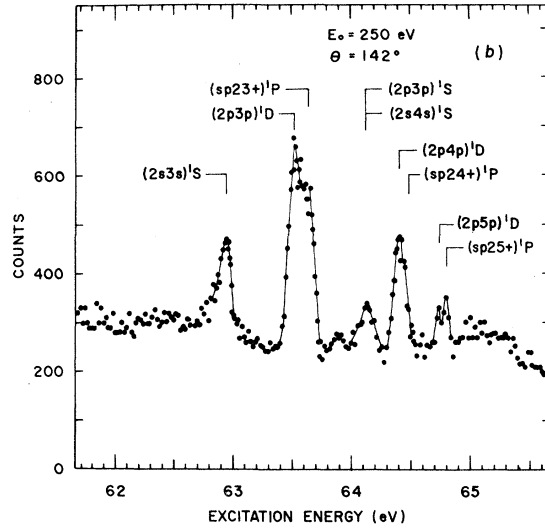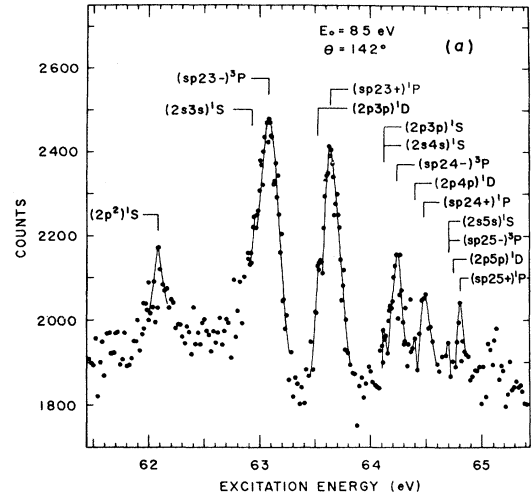| Impact energy (eV) | Single differential cross section (differential in angle only) $\sigma(\theta)$ $(10^{-21}$ cm^2/sr) | | | | | |
	$(2s^2)^1S$ 142°	$(2s2p)^3P$ 142°	$(2p^2)^1D$ 127°	$(2p^2)^1D$ 33°	$(2s2p)^1P$ 127°	$(2s2p)^1P$ 33°
1000	0.75		1.3		1.2	
250	4.4		5.0	0.13	4.5	1.6
210				0.27		1.8
180	4.9		6.5	0.67	5.2	2.9
150				1.5		4.6
130	5.8	0.36	6.6	1.9	5.4	4.8
100	3.8	0.74	3.4		4.1	
90				1.6		1.9
85	3.5	2.1	1.8		2.6	
75	3.9	3.2				
65		9.3				

FIG. 13. Energy spectra of electrons ejected from high-lying autoionization states in helium: (a) 85-eV electron impact; (b) 250-eV electron impact. Ejection angle is 142°; $\Delta E_{1/2} = 0.08$ eV. Energy positions of autoionization states identified in this work are shown in figures (a) and (b).

The single differential cross section $\sigma(\theta)$ may be interpreted as the differential excitation function of the autoionizing state when seen as a function of primary energy, and can be positive or negative, principally depending upon the value of q.[16,35] A positive value of $\sigma(\theta)$ corresponds to a peak of the resonance; a negative value, to a dip. In Fig. 11 are shown the single differential cross sections $\sigma(\theta)$ for the $(2s^2)^1S$, $(2s2p)^3P$, $(2p^2)^1D$, and $(2s2p)^1P$ states in the backward directions as a function of the primary energy, where the res-

TABLE II. Resonance energies (E_r's) of autoionization states in helium (in units of eV). The figures in brackets denote the expected error in the last digit of the experimental values.

State	Experiment (E_r)					Theory (E_r)					
	This work	Madden and Codling[a]	Rudd[b]	Hicks and Comer[c]	Siegbahn et al.[d]	Burke and Taylor[e]	Burke and McVicar[f]	Bhatia and Temkin[g]	Bhatia and Temkin[h]	Bhatia[i]	Altick and Moore[j]
$(2s^2)^1S$	57.84(2)		57.82(5)	57.82(4)	57.95(3)	57.842	57.865		57.844	57.830	
$(2s2p)^3P$	58.30(2)		58.34(5)	58.30(3)		58.317	58.360	58.298	58.321		
$(2p^2)^1D$	59.89(2)		60.0	59.89(3)	59.86(2)	59.911			59.915		
$(2s2p)^1P$	60.13	60.130(15) k	60.13	60.130	60.12(1)	60.149	60.269	60.143		60.145	60.340
$(2p^2)^1S$	62.08(3)		62.15(5)	62.06(3)		62.134	62.808		62.091		
$(2s3s)^1S$	62.94(3)		62.95(5)	62.94(3)	62.94(2)	62.975	63.009		62.962		
$(sp23-)^3P$ m	63.08(3)		63.08(5)	63.07(3)			63.141		63.107		
$(2p3p)^1D$	63.52(3)			63.50(3)	63.50(2)				63.526		
$(sp23+)^1P$	63.64(3)	63.651(7) l	63.65	63.65(3)	63.65(2)		63.691	63.677			63.707
$(2p3p)^1S$	64.12(3)		64.22(5)	64.18(3)			64.182		64.101		
$(2s4s)^1S$	64.12(3)		64.22(5)	64.23(3)	64.22(3)		64.216				
$(sp24-)^3P$ m	64.24(3)		64.22(5)				64.255				
$(2p4p)^1D$	64.40(3)			64.39(3)	64.38(3)						
$(sp24+)^1P$	64.48(3)	64.462(7)	64.46(5)	64.45(3)	64.45(2)		64.481		64.415		
$(2s5s)^1S$	64.70(4)		64.71(5)	64.67(4)	64.70(2)		64.698				
$(sp25-)^3P$ m	64.70(4)		64.71(5)				64.712				
$(2p5p)^1D$	64.74(4)			64.69(4)							
$(sp25+)^1P$	64.80(3)	64.813(7)			64.81(3)		64.824				

[a] Reference 1.
[b] Reference 7.
[c] Reference 26.
[d] Reference 23.
[e] Reference 47.
[f] Reference 46.
[g] A. K. Bhatia and A. Temkin, Phys. Rev. 182, 15 (1969).
[h] Reference 54.
[i] A. K. Bhatia, Phys. Rev. A 10, 729 (1974).
[j] P. L. Altick and E. N. Moore, Phys. Rev. Lett. 15, 100 (1965).
[k] This value was used to calibrate the energy scale of the present measurement.
[l] This value was used to calibrate the energy scale by Rudd (Ref. 7).
[m] These members $(sp2n-)^3P$ ($n = 3, 4, 5$) were identified as $(sp2n+)^3P$ by Hicks and Comer (Ref. 26). For details, see the text.

onance profiles of these states are predominantly Lorentzian. It will be seen from Fig. 11 that for backward directions the differential excitation functions for the $(2s^2)^1S$, $(2p^2)^1D$, and $(2s2p)^1P$ states have in common broad but pronounced maxima in the primary energy region from 100 to 200 eV and are all of the same order of magnitude, whereas that for the $(2s2p)^3P$ state rapidly decreases from a maximum near the threshold energy (58.3 eV) with increasing primary energy and becomes indiscernible at about 150 eV. The single differential cross sections for the $(2p^2)^1D$ and $(2s2p)^1P$ states seen at 33° are shown in Fig. 12 as a function of the primary energy for cases where the resonance profiles nearly look like the Lorentzian. We can see that the $\sigma(\theta)$ for the $(2p^2)^1D$ state at 33° is much smaller than that for the $(2s2p)^1P$ state over the whole energy range in contrast to the situation for backward directions. The cross-section values shown in Figs. 11 and 12 are summarized in Table I.

D. High-lying autoionization states

The autoionization states lying above ~ 62 eV in helium, which were observed previously by H_2^+ impact by Rudd[7] and recently by electron impact by Hicks and Comer,[26] have been also clearly observed in the present measurement. Two examples of energy spectra are shown in Fig. 13(a) for 85-eV electron impact and Fig. 13(b) for 250-eV electron impact, where the observed angle is 142° and the energy resolution is 0.08 eV in FWHM. While the identification of autoionization states was aided in the cases of H^+ and H_2^+ impacts by the fact that the triplet states are not excited by H^+ bombardment but show up strongly under H_2^+ bombardment, the energy spectra by electron impact can be identified by utilizing the fact that the intensity of each resonance line has a specific angular and impact energy dependence as already seen for autoionization states lying below ~ 62 eV; for example, the triplet states can be excited only by lower-energy electron impact. The energy spectrum by 85-eV impact [Fig. 13(a)] shows many optically as well as spin-forbidden autoionization states and is very similar to that by 75-keV H_2^+ impact.[7] On the contrary, the en-

ergy spectrum by 250-eV impact [Fig. 13(b)] seems rather simple and shows principally the singlet series of S, P, and D states. The energies of autoionization states of helium which we have measured are summarized in Table II, together with experimental values obtained by other workers and the results of theoretical calculations, where excitation energies of autoionization states lying below ~ 62 eV are also included.

The peak at 62.08 eV [see Fig. 13(a)] can be identified as the $(2p^2)^1S$ state because there is no other predicted level in this energy region. In the excitation energy region between 62.90 and 63.10 eV the existence of two autoionization states is expected; that is, $(2s3s)^1S$ and $(sp23-)^3P$. The peak at 62.94 eV for 250-eV impact [Fig. 13(b)] can be identified as the $(2s3s)^1S$ state, taking into consideration the fact that the angular dependence of the profile of this peak is very similar to that of the $(2s^2)^1S$ for the same impact energy and the peak for the $(2s2p)^3P$ state is indiscernible for 250-eV impact, especially for backward directions, as seen in Fig. 5. Furthermore, since the $(2s2p)^3P$ state is strongly excited for 85-eV impact as seen in Fig. 10(a), the peak at 63.08 eV for 85-eV impact [Fig. 13(a)] can be identified as the $(sp23-)^3P$ state. In the triplet ^3P case, the $n=2$ member of the $(sp2n+)^3P$ series is excluded on the Pauli principle. It is reasonable to consider that higher members of this series are quasiforbidden for excitation. Accordingly, it would be appropriate to assign the observed triplet $(sp2n)^3P$ series to be the "-" series. Following the procedure of assignment mentioned above and also taking into consideration the energies and widths of levels theoretically calculated, it is possible to assign the observed energies to members of the $(2sns)^1S$, $(2pnp)^1S$, $(sp2n-)^3P$, $(2pnp)^1D$, and $(sp2n+)^1P$ series as high as $n=5$ in the electron spectra of region extending up to ~65-eV excitation energy. Although many levels have been observed in the excitation energy region above ~65 eV as seen in Figs. 13(a) and 13(b), they have not been identified in this work mainly due to the overlapping of levels and the ambiguity on the level assignment. Our measured energies are in general in good agreement with previous experimental values and with some of theoretical calculations for $n=2$ to 5 series.

*On leave of absence from Department of Physics, Kyoto University, Kyoto, Japan.

[1] R. P. Madden and K. Codling, Astrophys. J. 141, 364 (1965).

[2] R. Whiddington and H. Priestley, Proc. Roy. Soc. A 145, 462 (1934).

[3] S. M. Silverman and E. N. Lassettre, J. Chem. Phys. 40, 1265 (1964).

[4] J. Arol Simpson, S. R. Mielczarek, and J. Cooper, J. Opt. Soc. Am. 54, 269 (1964).

[5] J. Arol Simpson, G. E. Chamberlain, and S. R. Mielczarek, Phys. Rev. 139, A1039 (1965).

[6] H. Boersch, J. Geiger, and B. Schröder, in *Physics of the One- and Two-Electron Atoms*, edited by B. Kleinpoppen (North-Holland, Amsterdam, 1969), p. 637.

[7] M. E. Rudd, Phys. Rev. Lett. 13, 503 (1964); 15, 580 (1965).

[8] M. E. Rudd and D. V. Lang, in *Proceedings of the Fifth International Conference on the Physics of Electronic and Atomic Collisions, Quebec 1965*, edited by L. Kerwin and W. Fite (Science Bookcrafters, Hastings-on-Hudson, N.Y., 1965), p. 153.

[9] A. Bordenave-Montesquieu, P. Benoit-Cattin, and D. Blanc, in *Proceedings of the Seventh International Conference on the Physics of Electronic and Atomic Collisions, Amsterdam 1971*, edited by L. M. Branscomb et al. (North-Holland, Amsterdam, 1971), p. 1041.

[10] A. Bordenave-Montesquieu and P. Benoit-Cattin, C. R. Acad. Sci. (Paris) B 272, 1473 (1971).

[11] A. Bordenave-Montesquieu and P. Benoit-Cattin, Phys. Lett. 36A, 243 (1971).

[12] N. Stolterfoht, Phys. Lett. 37A, 117 (1971).

[13] F. D. Schowengerdt and M. E. Rudd, Phys. Rev. Lett. 28, 127 (1972).

[14] N. Stolterfoht, D. Ridder, and P. Ziem, Phys. Lett. 42A, 240 (1972).

[15] A. Bordenave-Montesquieu, A. Gleizes, M. Rodiere, and P. Benoit-Cattin, J. Phys. B 6, 1997 (1973).

[16] F. D. Schowengerdt, S. R. Smart, and M. E. Rudd, Phys. Rev. A 7, 560 (1973).

[17] A. Bordenave-Montesquieu, P. Benoit-Cattin, A. Gleizes, and H. Merchez, J. Phys. B 8, L350 (1975).

[18] D. Burch, J. E. Bolger, and C. F. Moore, Phys. Rev. Lett. 34, 1067 (1975).

[19] D. Burch, J. E. Bolger, D. Schneider, and C. F. Moore, Phys. Rev. Lett. 36, 166 (1976).

[20] W. Mehlhorn, Phys. Lett. 21, 155 (1966).

[21] N. Oda, F. Nishimura, and S. Tahira, Phys. Rev. Lett. 24, 42 (1970).

[22] H. Suzuki, A. Konishi, M. Yamamoto, and K. Wakiya, J. Phys. Soc. Japan 28, 534 (1970).

[23] K. Siegbahn, C. Nordling, G. Johansson, J. Hedman, P. F. Hedén, K. Hamrin, U. Gelius, T. Bergmark, L. O. Werme, R. Manne, and Y. Baer, *ESCA Applied to Free Molecules* (North-Holland, Amsterdam, 1969), p. 26.

[24] H. Suzuki, Y. Jimbo, T. Takayanagi, and K. Wakiya, in *Proceedings of the Ninth International Conference on the Physics of Electronic and Atomic Collisions, Seattle 1975*, edited by J. S. Risley and R. Geballe (Univ. of Washington Press, Seattle, 1975), p. 763.

[25] E. Weigold, A. Ugbabe, and P. J. O. Teubner, Phys. Rev. Lett. 35, 209 (1975).

[26] P. J. Hicks and J. Comer, J. Phys. B 8, 1866 (1975).

[27] P. D. Burrow and G. J. Schulz, Phys. Rev. Lett. 22, 1271 (1969).

[28] J. T. Grissom, R. N. Compton, and W. R. Garrett, Phys. Lett. 30A, 117 (1969).

[29] P. D. Burrow, Phys. Rev. A 2, 1774 (1970).

[30] H. G. Berry, I. Martinson, L. J. Curtis, and L. Lundin, Phys. Rev. A 3, 1934 (1971).

[31] J. L. Tech and J. F. Ward, Phys. Rev. Lett. 27, 367 (1971).

[32] J. J. Quemener, C. Paquet, and P. Marmet, Phys. Rev. A 4, 494 (1971).

[33] G. Wiebes, Physica 48, 407 (1970).

[34] N. Oda, S. Tahira, and F. Nishimura, J. Phys. B 6, L309 (1973).

[35] S. S. Lipovetsky and V. S. Senashenko, J. Phys. B 5, L183 (1972); 7, 693 (1974).

[36] V. L. Jacobs, Phys. Rev. A 10, 499 (1974).

[37] F. H. Read, Radiation Res. 64, 23 (1975).

[38] N. Oda, F. Nishimura, and S. Tahira, Bull. Tokyo Instit. Techn. 96, 27 (1970).

[39] R. P. Madden and K. Codling, J. Opt. Soc. Am. 54, 268 (1964).

[40] N. Oda, F. Nishimura, and S. Tahira, J. Phys. Soc. Japan 33, 462 (1972).

[41] The peaks marked M and N for $E_0 = 65$ eV in Fig. 2 were identified to be due to electrons scattered inelastically after exciting the singly excited states, $(1sns)^1S$, ^3S or $(1snp)^1P$, ^3P, in helium, because the positions of maxima for these peaks move linearly with the energy of primary electrons. In particular, the peak marked N can be identified to the energy-loss peak corresponding to excitation of $n = 3$ states of helium, e.g., $(1s3s)^1S$, ^3S and $(1s3p)^1P$, ^3P, by measuring the energy difference between the peak N and the peak due to elastically scattered electrons. Since the energy of incident electrons is 65 eV and the excitation energy of $n = 3$ states is ~ 23 eV [that is, 22.9 eV for $(1s3s)^1S$ and 22.7 eV for $(1s3s)^3S$], the energy of electrons scattered after exciting these states is ~ 42 eV. On the other hand, the energy of electrons for peak N, when calculated by subtracting the first ionization potential (24.58 eV) from the excitation energy in the energy scale of Fig. 2, becomes ~ 38 eV. This result means that the energy scale determined from the peak energy of autoionized electrons cannot be applied to the kinetic energy for scattered electrons and the influence of the space charge in the collision region, as mentioned in Sec. II, on the energy shift is different between the scattered electrons and the autoionized ones.

[42] W. K. Peterson, C. B. Opal, and E. C. Beaty, J. Phys. B 4, 1020 (1971).

[43] W. K. Peterson, E. C. Beaty, and C. B. Opal, Phys. Rev. A 5, 712 (1972).

[44] C. B. Opal, E. C. Beaty, and W. K. Peterson, At. Data 4, 209 (1972).

[45] U. Fano and J. W. Cooper, Phys. Rev. 137, A1364 (1965).

[46] P. G. Burke and D. D. McVicar, Proc. Phys. Soc. (Lond.) 86, 989 (1965).

[47] P. G. Burke and A. J. Taylor, Proc. Phys. Soc. (Lond.) 88, 549 (1966).

[48] J. W. Cooper, S. Ormonde, C. H. Humphrey and P. G.

Burke, Proc. Phys. Soc. (Lond.) 91, 285 (1967).

[49]P. L. Altick and E. N. Moore, Proc. Phys. Soc. (Lond.) 92, 853 (1967).

[50]R. H. Perrott and A. L. Stewart, J. Phys. B 1, 381 (1968).

[51]C. S. Sharma and R. G. Wilson, Phys. Rev. 181, 39 (1969).

[52]P. G. Burke, in *Advances in Atomic and Molecular Physics*, edited by D. R. Bates and I. Estermann (Academic, New York, 1968), Vol. 4, p. 173.

[53]A. K. Bhatia, Phys. Rev. A 6, 120 (1972).

[54]A. K. Bhatia and A. Temkin, Phys. Rev. A 11, 2018 (1975).